Direct numerical simulation of reacting scalar mixing layers

S. M. de Bruyn Kops,[a] J. J. Riley, and G. Kosály

Department of Mechanical Engineering, University of Washington, Box 352600, Seattle, Washington 98195-2600

Understanding the passive reaction of two chemical species in shear-free turbulence with order unity Schmidt number is important in atmospheric and turbulent combustion research. The canonical configuration considered here is the reacting scalar mixing layer; in this problem two initially separated species mix and react downstream of a turbulence generating grid in a wind tunnel. A conserved scalar in this flow is, with some restrictions, analogous to temperature in a thermal mixing layer, and considerable laboratory data are available on the latter. In this paper, results are reported from high resolution, direct numerical simulations in which the evolution of the conserved scalar field accurately matches that of the temperature field in existing laboratory experiments. Superimposed on the flow are passive, single-step reactions with a wide range of activation energies and stoichiometric ratios (r). The resulting data include species concentrations as a function of three spatial dimensions plus time, and statistical moments and spectra of all species. Several aspects of the flow are investigated here with the conclusions that (1) reactions in which $r \neq 1$ are more accurately modeled by frozen and equilibrium chemistry limits than are reactions in which $r = 1$, (2) an existing definition of a reduced Damköhler number that includes temperature and stoichiometry effects is a useful measure of reaction rate, and (3) existing theoretical models for predicting the coherence and phase of fuel-oxidizer cross-spectra and the spectrum of the equilibrium fuel mass fraction when $r = 1$ yield accurate predictions. © *2001 American Institute of Physics.*
[DOI: 10.1063/1.1359185]

I. INTRODUCTION

The passive reaction of two scalars with order unity Schmidt numbers in shear-free turbulence is of interest to researchers studying chemical reactions in natural and engineering flows. The connection with the reactions that occur in the atmosphere, for instance, is readily apparent, since the species concentrations are so low in these natural processes that the heat released by the associated reactions has little effect on the surrounding flow. Even in fields of study in which the hydrodynamic problem cannot be decoupled from the chemical processes, the passive case is interesting since it involves aspects of mixing which must be accounted for in theories of scalar transport and reaction, while being relatively easy to study.

A canonical configuration for two species streams reacting in a turbulent flow is the reacting scalar mixing layer. Fuel and oxidant are introduced through separate halves of a turbulence generating grid in a wind tunnel, and transport and reaction occur in decaying, homogeneous, isotropic turbulence; the configuration is shown schematically in Fig. 1, and the coordinate system and various quantities are defined there for reference.

Bilger *et al.*[1] and Li *et al.*[2] examine the reacting scalar mixing layer via wind tunnel experiments with ozone and nitric oxide as the reactants. As noted by Bilger *et al.*, the experiments ''represent a compromise between the desire for high Reynolds numbers, large distance downstream, Damköhler numbers in the range near unity, degree of spatial resolution and cost of construction and operation,'' and so the measurements are taken in developing and highly anisotropic turbulence. There remains a need for additional data on this flow, but the problem of generating and measuring a well-developed reacting mixing layer in the laboratory is not significantly easier than it was when the measurements just cited were taken.

When the molecular diffusivities and densities of the reacting species are equal, the reacting scalar mixing layer is analogous in many respects to a thermal mixing layer in which temperature is replaced by the mixture fraction[3] as the scalar. A nearly ideal thermal mixing layer is easier to measure experimentally than is the reacting case, and it has been studied extensively by Watt and Baines,[4] Libby,[5] LaRue and Libby,[6] LaRue *et al.*,[7] Ma and Warhaft,[8] and Gibson *et al.*[9] Recently, de Bruyn Kops and Riley[10] reported an accurate numerical simulation of the experiment by Ma and Warhaft, which augments the laboratory data with a high resolution description of the velocity and scalar fields as a function of three spatial dimensions plus time. Running simulations that reproduce the results from specific wind tunnel experiments, rather than performing numerical experiments which compare only qualitatively with the laboratory counterparts, produces very detailed and highly credible data sets. Additional phenomena can then be numerically introduced into the ex-
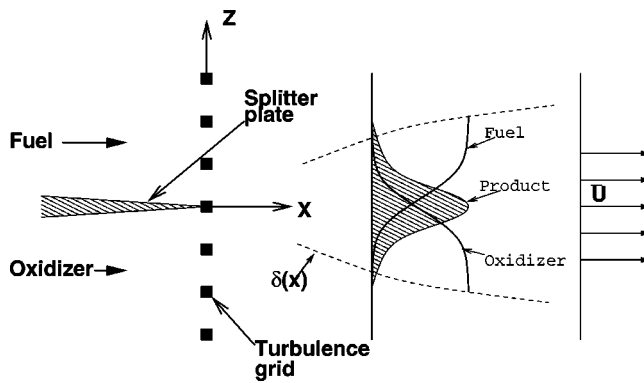
---

[a]Electronic mail: debk@u.washington.edu

FIG. 1. Schematic of a reacting mixing layer.

periment, e.g., superimposing a passive reaction on a thermal mixing layer, with high confidence that, if the simulations are shown to be numerically accurate, the resulting data sets correctly reflect the physics and chemistry being studied. The report of simulations in which passive reactions have been added to an accurate simulation of a thermal mixing layer to yield data sets for a nearly ideal reacting mixing layer is the subject of this paper.

II. REACTION MECHANISM

It is important to select problems for study which involve relevant physical phenomena, but which can be adequately explored with the tools available. It is often equally important to limit the number of phenomena being studied in order to be able to identify the effects of a particular physical process. The direct numerical simulations in the current research are designed to be highly accurate, but computational power and the desire to isolate the effects of particular phenomena severely limit the complexity of the chemical reactions and flow configurations that are simulated. In particular, the chemical reactions are limited here to two dilute species and a one-step, irreversible reaction,

$$F + rO \rightarrow (1+r)P, \tag{1}$$

with both isothermal and temperature dependent reaction rates. The isothermal case is the same physical problem that was considered by Bilger et al.[1] and Li et al.[2] The assumption of dilute species allows the combustion and hydrodynamic problems to be decoupled, i.e., the density, kinematic viscosity, and molecular diffusivities are constant; allowing the fluid properties to vary with temperature in a simulation of decaying turbulence that starts at moderate Reynolds number can result in regions of laminar flow, which are not of interest in this work. The assumption of a single reaction greatly simplifies the chemical kinetics and reduces the computational costs. While it is assumed that the fluid properties are constant, temperature effects are provided for through the reaction rate terms, e.g., $\dot{w}_F = -A Y_F Y_O \exp(-T_a/T)$ is the production rate of the fuel mass fraction. Here, A is the reaction rate constant, Y_F and Y_O are the mass fractions of fuel and oxidant, T_a is the activation temperature, and T is the local temperature, which can be expressed in terms of the mixture and mass fractions.[11] Two other important tempera-

tures are the adiabatic flame temperature, T_f, and the (equal) temperatures of the fuel and oxidizer streams, T_∞.

The reaction kinetics can be characterized by the quantities $\alpha = (T_f - T_\infty)/T_f$, $\beta = \alpha T_a/T_f$, and $T_r = (T - T_\infty)/(T_f - T_\infty)$;[12] α is a heat release factor, β is a dimensionless activation energy, and T_r is a reduced temperature. The species source terms can be written in terms of these quantities as, e.g.,

$$\dot{w}_F = -A \exp\left(\frac{-\beta}{\alpha}\right) Y_F Y_O \exp\left[\frac{-\beta(1-T_r)}{1-\alpha(1-T_r)}\right]. \tag{2}$$

This formulation leads to a convenient definition of a global Damköhler number,

$$Da \equiv \frac{AL}{u_{rms}} \exp(-\beta/\alpha), \tag{3}$$

where u_{rms} is the average of the rms velocity fluctuations (u, v, and w) and L is the integral length scale. In the case of high β, asymptotic methods can be used to derive a chemical time scale of the diffusion flame,[13–15] which leads to a reduced Damköhler number defined at the stoichiometric surface:

$$Da_T \equiv \frac{rA\xi_{st}e^{-T_a/T_f}}{\chi_{st}/2}\left[\frac{T_f^2}{T_a(T_f-1)}\right]^3 [2\xi_{st}(1-\xi_{st})]^2. \tag{4}$$

Here, ξ_{st} and χ_{st} are the mixture fraction and its dissipation rate at the stoichiometric surface and r is the mass of oxidant that consumes unit mass of fuel. Averaging Da_T at all points where $\xi = \xi_{st}$ yields a global, temperature dependent Damköhler number denoted $\langle Da_T \rangle$.

It should be noted that the mixture fraction (ξ) used in this work is defined as by Bilger:[3]

$$\xi = \frac{rY_F - Y_O + Y_O^\infty}{rY_F^\infty + Y_O^\infty}, \tag{5}$$

where the superscript ∞ indicates the mass fractions in the unmixed fuel and oxidant streams. Inherent in this definition is the assumption that the mass diffusivities of all species are equal. It also assumed here that the Lewis number of all species is unity so that the local temperature can be related to the species mass fractions. Also, the mixture fractions of the fuel and oxidizer streams are taken to be one and zero, respectively; this does not restrict the application of the methodology, however, since any two-stream, nonpremixed reacting flow problem with diluent can be mapped to a no-diluent case by adjusting A and r.

III. LABORATORY EXPERIMENTS

In the experiments conducted at The University of Sydney,[1,2] hereafter the Sydney experiments, a nitric oxide-ozone mixing layer approximates the irreversible, isothermal mechanism of (1) evolving in grid turbulence, and velocity and scalar statistics are collected between 12 and 21 mesh widths downstream of the turbulence generating grid. Two values of the stoichiometric ratio (r) are considered (approximately unity, and approximately 0.45), and the reactants are diluted with various amounts of air. The result is a

TABLE I. Gross properties of the laboratory scalar mixing layer velocity fields. The velocity data of Bilger *et al.* (Ref. 1) are in error (Ref. 17). The data in this table have been corrected.

	LaRue *et al.* (1981)	Ma and Warhaft (1986)	Bilger *et al.* (1991)
x/M		100	12
U(cm/s)	780	620	50
u/U		0.014	0.080
w/U		0.012	0.040
ϵ(cm^2/s^3)		361	2.40
M(cm)	4	2.50	32
L(cm)		1.66	17.0
λ(cm)		0.620	2.708
η_k(cm)		0.0549	0.324
$Re_M = UM/\nu$	21010	9394	11700
$Re_L = u_{rms}L/\nu$		84.8	455
$Re_\lambda = u_{rms}\lambda/\nu$		32.7	72.5
Test section x/M	21–67	62.4–132.4	12–21

set of experiments with nominally two different reaction rates, which can be characterized as moderate and fast (but finite), based on comparisons of the mean reactant concentration profiles with those of the equilibrium and frozen chemistry limits. Note that the turbulence decays, and the Damköhler number increases, with downstream distance so that each experiment actually represents a range of Damköhler numbers.

While the simple reaction in the Sydney experiments is well suited for direct numerical simulation (DNS), due to experimental considerations the test section in the wind tunnel is upstream of where grid turbulence is generally considered to be well developed,[16] and the velocity field is highly anisotropic, making it difficult to reproduce the experimental conditions in a numerical simulation. Numerical experiments, however, are not subject to the same restrictions as those performed in the laboratory, and passive reactions with a wide range of stoichiometric ratios, reactions rates, and activation temperatures can be numerically superimposed on a simulation of a scalar mixing layer which exhibits the characteristics of a laboratory experiment of a thermal mixing layer in fully developed, homogeneous, isotropic turbulence. To ensure that the velocity and passive scalar fields are accurately simulated, it is advantageous to match the simulations with existing laboratory experiments. This is the approach taken in the current research.

Many of the laboratory experimentalists, cited in Sec. I, who studied the thermal mixing layer present results of earlier works in addition to their own, and discuss differences in the various sets of data. From these discussions, it is apparent that the experiments of LaRue and Libby,[6] LaRue *et al.*,[7] and Ma and Warhaft[8] are the most refined, and are in close agreement with each other. Of these, the experiment of Ma and Warhaft is at a Reynolds number most suitable for direct numerical simulation on the available computers, and, for this reason only, it forms the basis for the numerical experiments discussed in this paper. Various properties of the laboratory data are given in Table I where u and w are the streamwise and transverse rms velocity fluctuations, U is the mean streamwise velocity, ϵ is the turbulence kinetic energy

dissipation rate, M is the spacing of the turbulence generating grid, λ and η_k are the Taylor and Kolmogorov length scales, and ν is the kinematic viscosity.

IV. NUMERICAL EXPERIMENTS

A. Velocity fields

The direct numerical simulation method used in this research is the same as that used by de Bruyn Kops and Riley[18] to accurately simulate the decaying isotropic turbulence experiments of Comte-Bellot and Corrsin.[19] The simulations reported here are also discussed by de Bruyn Kops and Riley.[10] Briefly, a massively parallel, pseudospectral code advances the momentum and scalar transport equations in time, with all the dynamically relevant large and small scales fully resolved. A second-order Adams–Bashforth scheme with projection is used for time stepping. The simulations are run in two computational domains: (1) $512\times512\times1024$ grid points with periodic boundary conditions in all directions, and (2) 512^3 grid points with periodic boundary conditions in the x and y directions and a free-slip boundary condition in the z direction, that of the mean scalar gradient. With respect to the experiments of Ma and Warhaft, the physical size of the larger computational domain is $25.1\times25.1\times50.3$ cm. Taylor's hypothesis is invoked to relate simulation time to wind tunnel downstream distance so that the numerical and laboratory experiments can be directly compared; temporal averaging in the laboratory corresponds to spatial averaging in the simulations. In this work, the velocity and conserved scalar fields in the simulations are designed to closely resemble those in the laboratory experiments of Ma and Warhaft,[8] but Ma and Warhaft do not provide energy spectra, and so the simulations cannot be exactly matched to the laboratory data. Velocity field data, in addition to those presented by Ma and Warhaft,[8] are given by Sirivat and Warhaft.[20]

The scheme of de Bruyn Kops and Riley[18] was used to initialize the flow field. The process yields a velocity field with well-developed turbulent structures and with a desired kinetic energy spectrum. In the current research, only the length scales of the laboratory data are known, not the entire spectrum. Therefore, an equation for the three-dimensional kinetic energy spectrum, $E(k)$, is assumed, which approximately matches the spectrum of Comte-Bellot and Corrsin.[19] This spectrum, obtained by combining the theoretical form for the low-wave number production range derived by Tennekes and Lumley,[21] the well-known $k^{-5/3}$ spectrum in the inertial range, and the form for the high-wave number dissipation range first derived by Corrsin,[22] is

$$E(k) = A \exp(Bk^{-4/3})k^{-5/3}\exp(Ck^{4/3}) . \tag{6}$$

The coefficients were adjusted in order to match the estimated laboratory rms velocity (u_{rms}) and integral length (L) at $x/M=20$ (Ma and Warhaft report exact values for these parameters only at $x/M=100$), where M is the spacing of the turbulence generating grid. The simulation was advanced to $x/M=200$ and the decay laws $L \propto [(x-x_0)/M]^m$ and $u_{rms} \propto [(x-x_0)/M]^{m-1}$ were fitted to the resulting data. Next, the observation that the energy spectrum of decaying, isotropic,
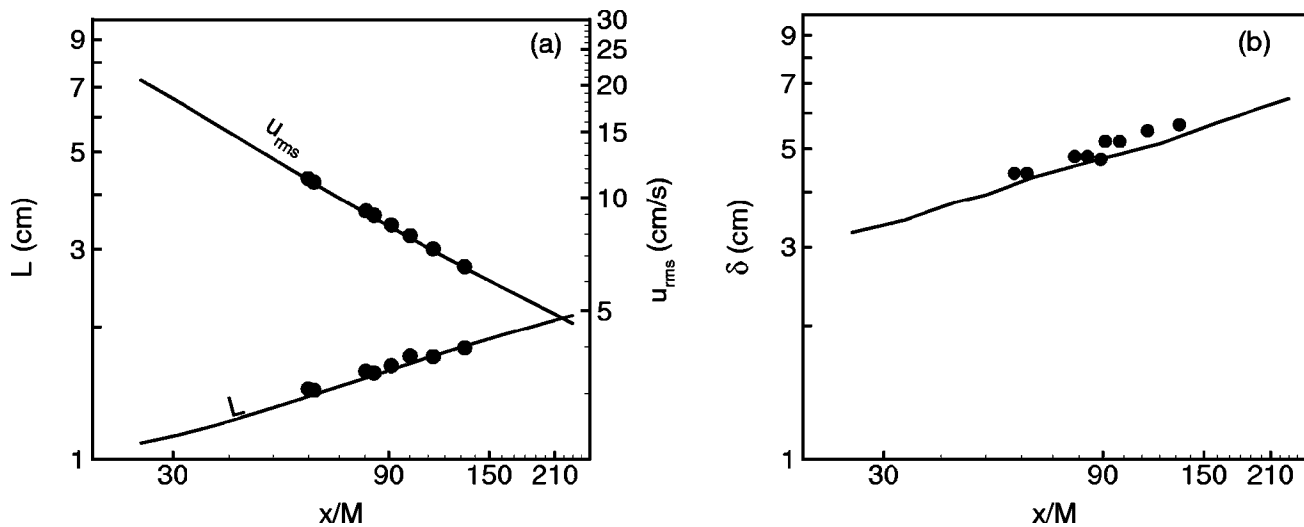
FIG. 2. Properties of the velocity and scalar fields for the mixing layer.

homogeneous turbulence evolves in an approximately self-similar manner was used to form a new initial spectrum based on the DNS spectrum at $x/M = 200$, and the simulation run again. This process was repeated, with small adjustments to the initial spectrum and Reynolds number, until u_{rms} and L at $x/M = 100$ and m were matched. The gross properties of the velocity field are compared with the laboratory data in Fig. 2(a).

B. Mixture fraction field

The mixture fraction field (ξ) and a fuel mass fraction field (Y_F) were superimposed on the simulated velocity field in order to simulate the reaction of (1). With the assumption that all Lewis numbers equal unity, the remaining mass fractions and the temperature can be related to ξ and Y_F. The mixture fraction field was initialized with an error function and allowed to evolve with the velocity field from $x/M = 25.4$ to $x/M = 33.5$. The resulting scalar field was reintroduced into the velocity field at $x/M = 25.4$, the simulation advanced to $x/M = 33.5$, and the process repeated until the width of the mean field equaled that estimated for the laboratory experiment, and the virtual origin of the scalar field coincided with that of the velocity field. The resulting scalar field has the desired large scale properties and is roughly synchronized with the velocity field. The intent was to have a physically reasonable scalar field at $x/M = 62.4$, the location of the first laboratory data. The widths of the mixing

layer (δ) in the simulation and laboratory fields are compared in Fig. 2(b). Extensive comparisons between the laboratory and simulated scalar fields (scalar flux, mean scalar, second, third, and fourth moments of the scalar fluctuations) demonstrate that the simulated conserved scalar field is consistent with that in the laboratory experiments for all statistics considered.[10]

C. Mass fraction fields

Three sets of reacting scalar mixing layer simulations are analyzed in this research: isothermal with $r = 1$, temperature dependent with $r = 1$, and temperature dependent with $r \neq 1$. The parameters for each simulation are listed in Table II. The fuel fields in the isothermal cases were initialized at $x/M = 25.4$ with the quasistationary flamelet (QFL) solution,[23]

$$-\frac{\chi}{2}\frac{\partial^2 Y_F}{\partial \xi^2} = -A Y_F Y_O. \tag{7}$$

In the temperature dependent cases, the fuel fields were initialized with the near-equilibrium chemistry solution (the equilibrium chemistry solution spatially filtered to be resolved on the numerical grid). The near equilibrium solution is used to initialize the fuel fields instead of the QFL solution in the cases with Arrhenius kinetics for two reasons: (1) to ensure that the reaction zone is hot enough to sustain burning over a broad range of Damköhler numbers as the simulations

TABLE II. Reaction parameters.

	α	β	r	Da initial	Da final	$\langle Da_T \rangle$ at $x/M = 50.1$	n_r at $x/M = 50.1$
ML1	⋯	0	1	0.22	2.6	⋯	⋯
ML2	⋯	0	1	0.66	8.0	⋯	⋯
ML3	0.88	5.4	1	17.8	215	0.79	26
ML4	0.88	5.4	1	75.7	914	3.2	16
ML5	0.88	5.4	1	302	3659	13	10
ML6	0.88	2.6	10	53.6	647	4.3	14
ML7	0.88	2.6	30	53.6	647	0.66	27

undergo transients at very early times due to the initial conditions, and (2) to ensure that the initial condition is well defined and reproducible by other researchers. These two points are discussed in the following paragraphs.

Despite the iterative technique for synchronizing the initial scalar and velocity fields, discussed in Sec. IV B, adjustment of the scalar field to the velocity field very early in the simulations results in steep local gradients of the mixture fraction, which can lead to extinction. Also, the QFL solution is computed locally, and is not necessarily sufficiently smooth in physical space; using it as an initial condition leads to transients in the mass fractions and reactions rates which are dependent on the local initial conditions, and which provide little or no information about physical flames. In isothermal or vigorous temperature dependent reactions, these transients can usually be ignored; in less vigorous temperature dependent reactions, they can extinguish a flame that would otherwise burn if the initial transients were eliminated. In order to study nonisothermal reactions with very high and very low Damköhler numbers using a consistent initialization method, the equilibrium limit is used in this research.

D. Kinetics

To provide an overview of the relative reaction rates and amount of extinction in the simulated reactions, scatter plots of the product mass fractions (Y_P) versus the mixture fraction (ξ) for the cases where $r=1$ are shown in Fig. 3, and for the cases where $r \neq 1$ in Fig. 4.

In the top two plots in Fig. 3, it is apparent that the reaction rate is low in case ML1 and moderate in case ML2, based on the separation of the clouds of points from the equilibrium limit. The lower four panels in Fig. 3 are for three cases with temperature dependent kinetics (ML3, ML4, ML5), with case ML4 shown at two different downstream locations, and thus two different values of $\langle \mathrm{Da}_T \rangle$. In case ML3, there is considerable mixing without burning, either due to extinction or nonignition, and tests indicate that reducing A by a factor of 2 from what it is in the ML3 case results in global extinction. In case ML5, the reaction rate is about 17 times higher than it is in case ML3; the reaction occurs at the equilibrium rate in most locations at $x/M = 50.1$ (shown), and at virtually all locations at $x/M = 231$ (not shown). Thus, cases ML3 and ML5 bracket the full range of reaction rates from very low to near equilibrium.

In Fig. 5 the unscaled profiles of the average product mass fraction for simulations ML3 and ML5 are shown.

The profiles are generated by averaging the mass fraction fields over xy planes. Both cases start with the same equilibrium chemistry condition, but the product advects and diffuses faster than it is created in case ML3, while being created faster than it advects and diffuses in case ML5.

ML4 is a nonisothermal case with intermediate reaction rate. The simulations are designed so that $\langle \mathrm{Da}_T \rangle$ is the same in ML4 at $x/M = 50.1$ and ML3 at $x/M = 231$, and is also the same in ML4 at $x/M = 231$ and ML5 at $x/M = 50.1$. So it is possible to observe the flow at the same $\langle \mathrm{Da}_T \rangle$ but different Reynolds numbers. The reactants mix in a nearly self-similar

manner,[10] so, by examining the scatter plots of Y_P vs ξ at the same $\langle \mathrm{Da}_T \rangle$ but different x/M, the applicability of $\langle \mathrm{Da}_T \rangle$ as a measure of reaction rate can be evaluated. Such a comparison is made in the bottom two panels of Fig. 3. The two plots are very similar, with ML4 appearing to be slightly closer to the equilibrium limit than ML5. A more detailed comparison of the two fields is made in Fig. 6, in which are plotted the conditional averages of the product mass fractions for each field, and the square of the fluctuations about the average, $Y_P'^2$, where $Y_P' = Y_P - \langle Y_P | \xi \rangle$. The mass fraction averages and the fluctuations are nearly the same in both fields.

The conclusion is that $\langle \mathrm{Da}_T \rangle$ is a useful measure of the reaction rate in these simulations, especially given the number of factors which effect the characteristic time scale of a temperature dependent reaction.

The remaining two simulations, ML6 and ML7, involve temperature dependent chemistry at a lower activation temperature than ML3 through ML5. Also, r is much greater than unity so that the peak reaction rate does not coincide with the centerline of the mixing layer. Some evidence of extinction is apparent in Fig. 4 for both cases, with ML7 having a less vigorous reaction than ML6.

E. Spatial and temporal resolution

The small scale resolution requirement for the velocity and conserved scalar (with order one Schmidt number) fields in a simulation of isothermal, incompressible turbulence is well established to be $k_{\max} \eta_k \geqslant 1$, where $k_{\max}$ is the largest wave number in the simulations and η_k is the Kolmogorov length scale.[24] More recently, de Bruyn Kops and Riley[18] showed that, for simulations of turbulence downstream of a grid, the transfer rate of energy from the largest resolved scale should be approximately zero in order for the large eddies in the flow to develop as they do in a wind tunnel. Since the current simulations involve a passive scalar in incompressible turbulence, both of these resolution criteria apply, and both are met, with $k_{\max} \eta_k$ ranging from 1.6 to 5.7 and the ratio of the largest to the smallest wave numbers equal to 240.

Demonstrating adequate resolution of the reacting scalar is more difficult. In the limit of infinite Damköhler number, the reaction between initially segregated fuel and oxidizer will occur in infinitesimally thin regions as fast as the two species are mixed, which implies that direct numerical simulations of nonpremixed combustion are limited with respect to the Damköhler number of the simulated reactions.[25] Reaction mechanisms with multiple steps, reaction rates that are dependent on temperature, and coupling between the reaction process and the fluid dynamics all complicate the problem of spatial resolution. Mell *et al.*[26] provide Damköhler numbers suitable for high resolution pseudospectral DNS with one-step chemistry, but only for the case of zero activation temperature. Montgomery[27] indicates that resolution of the reaction rate limits the strain rates that can be allowed in an accurate simulation with multistep, temperature dependent reactions, and coupling between the temperature and velocity fields. Mahalingam *et al.*[28] report DNS results for
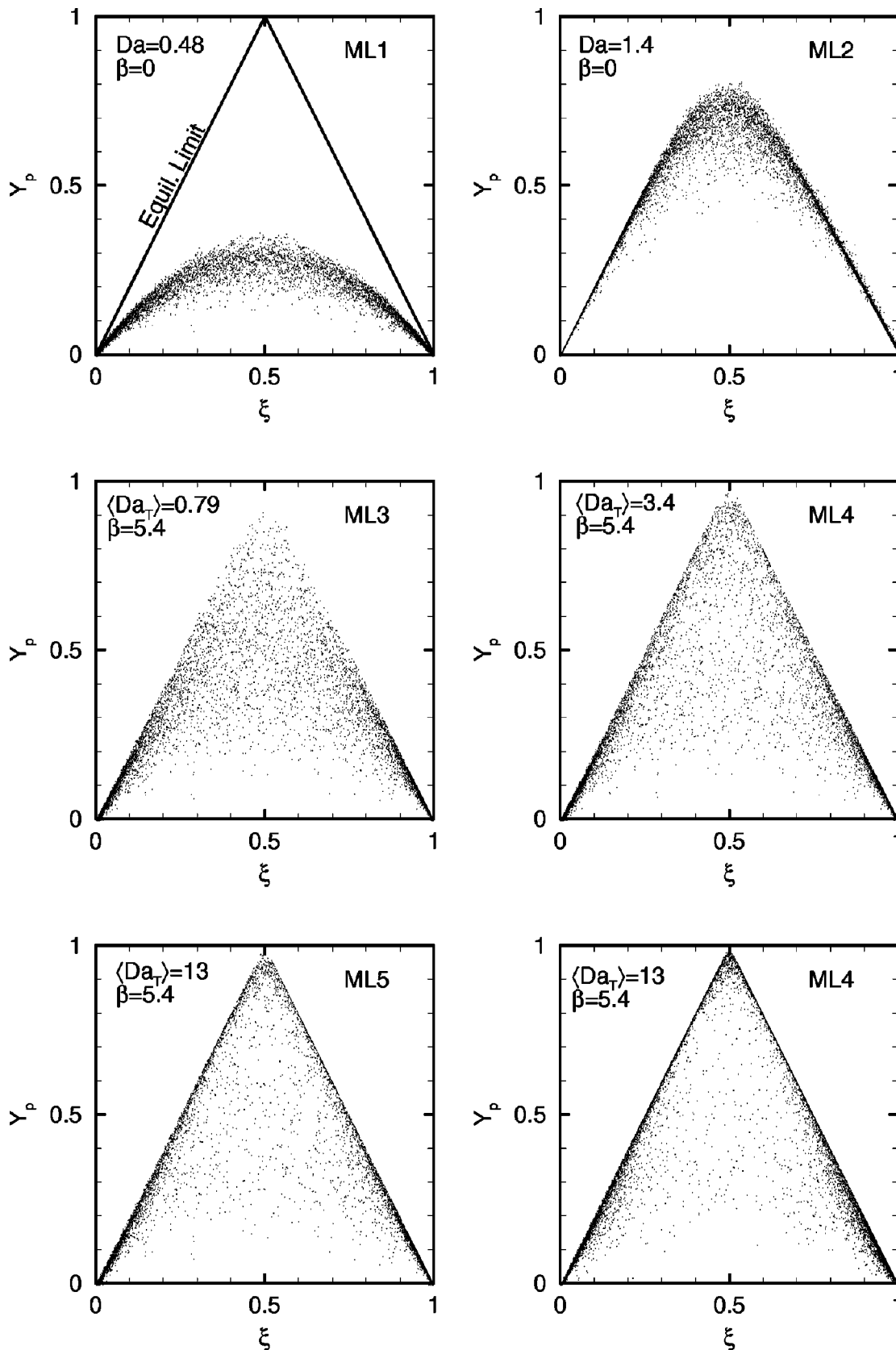
FIG. 3. Scatter plots of Y_P vs ξ for the mixing layer cases with ($r=1$).

single- and two-step reaction mechanisms with large activation temperatures and temperature dependent viscosities, densities, and diffusivities, but do not discuss the resolution of the calculations. Swaminathan and Bilger[29] and Bushe

et al.[30] modified multiple-step reaction mechanisms in efforts to increase the size of the flame structures so that they would be easier to resolve numerically, without significantly changing other aspects of the combustion.
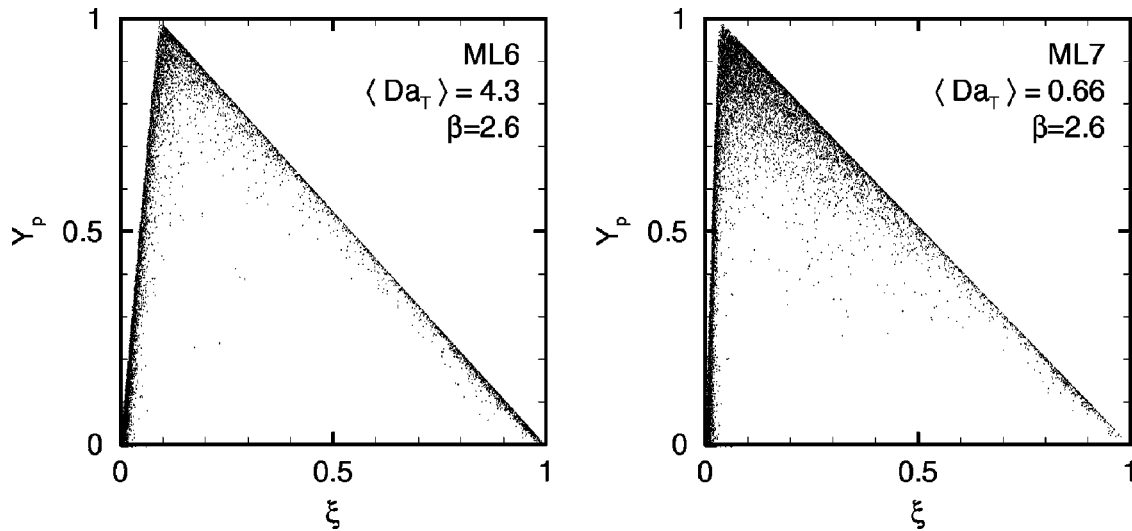
FIG. 4. Scatter plots of Y_P vs ξ for the mixing layer cases with ($r \neq 1$).

Lee and Pope[31] conducted a careful study of spatial accuracy requirements for a scalar which is the perturbation of the product mass fraction from its equilibrium chemistry value. The transport equation for this scalar includes a micromixing term proportional to the scalar dissipation rate (χ) times the second derivative with respect to ξ of the equilibrium product mass fraction. The authors show that this micromixing term and the reaction source term dominate the diffusion and convection terms and limit the resolution of the simulation. Since the transport equation for Y_F contains no term comparable to the micromixing term, the resolution of

the simulations in this research are expected to be limited by the reaction rate, just as in the simulations of Montgomery.[27]

Vervisch and Poinsot[32] approach the question of resolution by estimating the thickness of the reaction zone and of the diffusive layer surrounding it, and derive the following resolution criteria:

$$\mathrm{Re}_L < \left(\frac{N}{n_l}^{4/3}\right), \quad (\langle \xi'^2 \rangle \mathrm{Re}_L)^{1/2} \mathrm{Da}_T^{1/3} < \left(\frac{N}{n_L n_r}\right). \tag{8}$$

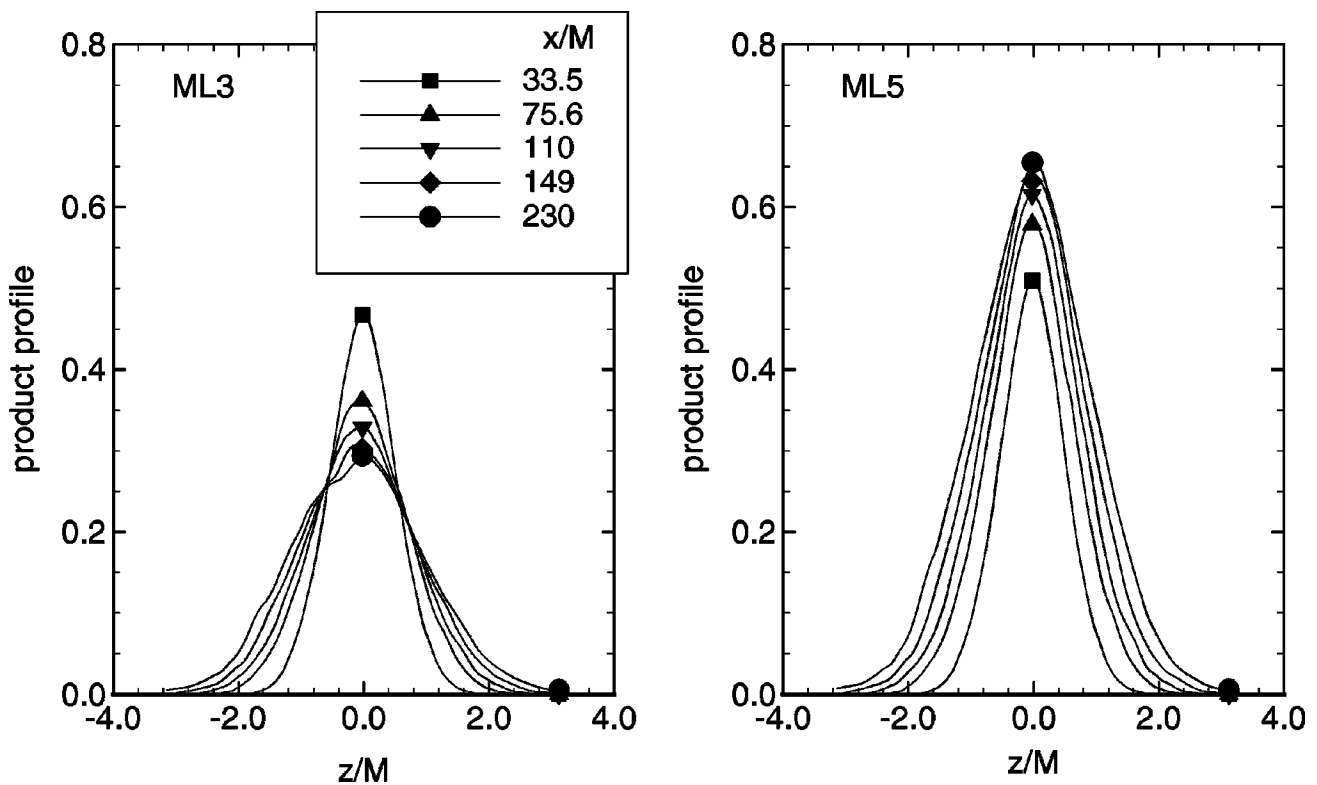Here, Re_L is the Reynolds number based on the rms velocity

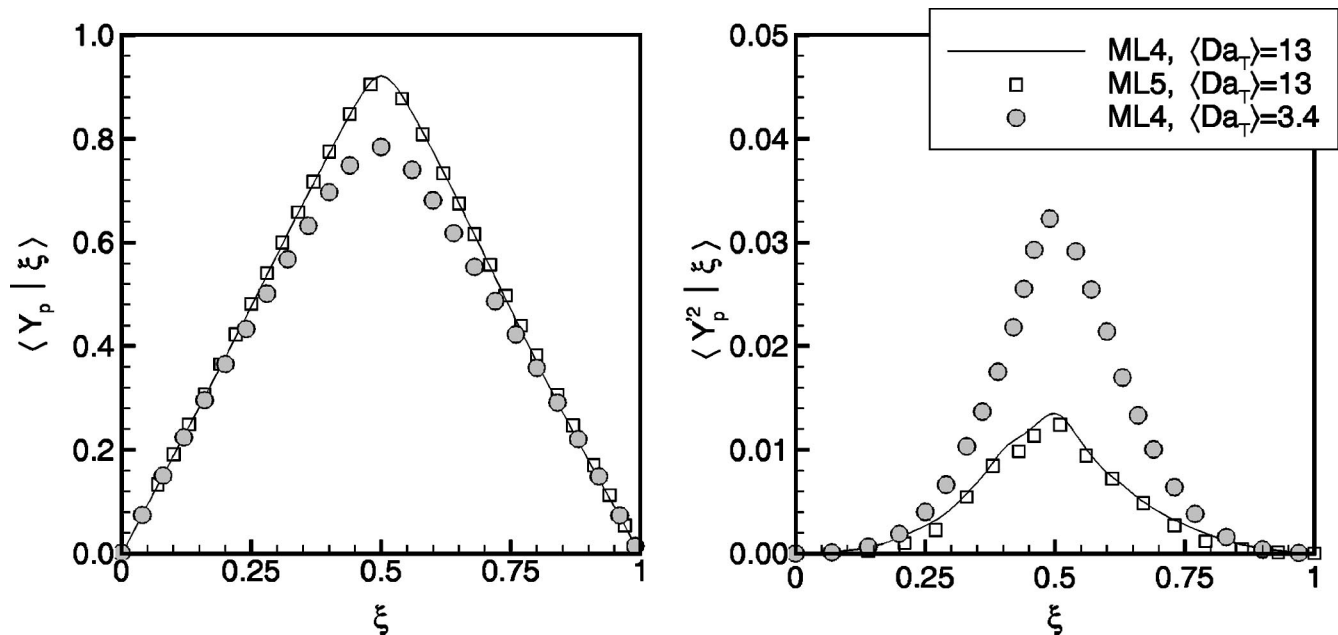FIG. 5. Product mass fraction profiles for cases M3 and M5.

FIG. 6. Conditional averages of product mass fraction, and the fluctuations about the average, for cases ML4 and ML5 with $\langle \mathrm{Da}_T \rangle = 13$, and for case ML4 with $\langle \mathrm{Da}_T \rangle = 3.4$.

and the integral length scale, N is the number of points in one direction of the numeric grid, n_r is the number of points necessary to resolve the reaction zone, and n_L is the number of integral length scales contained within the numerical domain. The first criterion is equivalent to $k_{max}\eta_k > 2\pi$, which is considerably more restrictive than that of Eswaran and Pope.[24] Both criteria rely on estimates for several length and time scales, and therefore are not expected to be exact measures of resolution. Values of n_r in the simulations are given in Table II.

While the cited literature suggests a starting point for determining the small-scale resolution requirements of a simulation with combustion, it does not provide a readily accepted rule of thumb such as that developed by Eswaran and Pope[24] for the nonreacting case. Also, the grid spacing required in a simulation depends to an extent on the statistics of interest; e.g., Nilsen and Kosály[33,34] increased the resolution of existing simulations of Mell et al.,[26] which are accurate for the physical phenomena being studied by the latter, in order to explore the small-scale phenomena of differential diffusion. Finally, due to the nonlinear nature of turbulence, for any practical numerical grid spacing there will likely be isolated regions in the velocity and scalar fields that are poorly resolved; the issue is not whether they exist, but whether they affect the statistics of interest.

In the current research, the spatial resolution of the simulations was determined to be adequate by the following process. First, the criteria of Eswaran and Pope[24] and de Bruyn Kops and Riley[18] were applied to determine that a numerical grid with $320 \times 320 \times 640$ points is appropriate for nonreacting simulations; then the inert case was run using the initialization procedure described in Sec. IV A, and the velocity and scalar field results were found to be consistent with the laboratory data. Next, the simulations with reaction were advanced to $x/M = 231$ in the 512^3- or $512 \times 512 \times 1024$-point

domain and the fields were analyzed visually at various downstream locations. Visual analysis was focused on the locations where the gradient of the reaction rate was high, based on the above-cited literature which indicates that this source term is the most difficult term to resolve in the mass fraction transport equations. Isolated regions of questionable resolution, as indicated by the reaction rate oscillating with the highest resolved frequency, were observed, but appeared to be no more prevalent than similar oscillations in the velocity field, which is very well resolved by the criterion of Eswaran and Pope.[24] Finally, portions of the reacting scalar simulations were run using a computational domain having 600^3 grid points, and compared with those run in the domain with 512^3 grid points; there was negligible difference between the mean, variance, skewness, and kurtosis profiles of the reaction rate in the two domains. The conclusion is that the simulations are adequately resolved spatially for the phenomena reported in this paper.

Temporal resolution was determined to be adequate by running portions of each simulation with two different time steps, which differ by a factor of 2, and noting no significant differences in the results. Parts of several simulations were also computed using a third-order Adams–Bashforth algorithm, without altering the time step, and again no differences were noted.

V. DISCUSSION

In this section, the simulation data are compared qualitatively with the Sydney experiments for the isothermal cases with $r = 1$; new results for the nonisothermal reactions and reactions in which the stoichiometric mixture fraction (ξ_{st}) is not equal to 0.5 are also presented. The volume of data from the simulations is overwhelming when results from all available downstream locations are considered, so
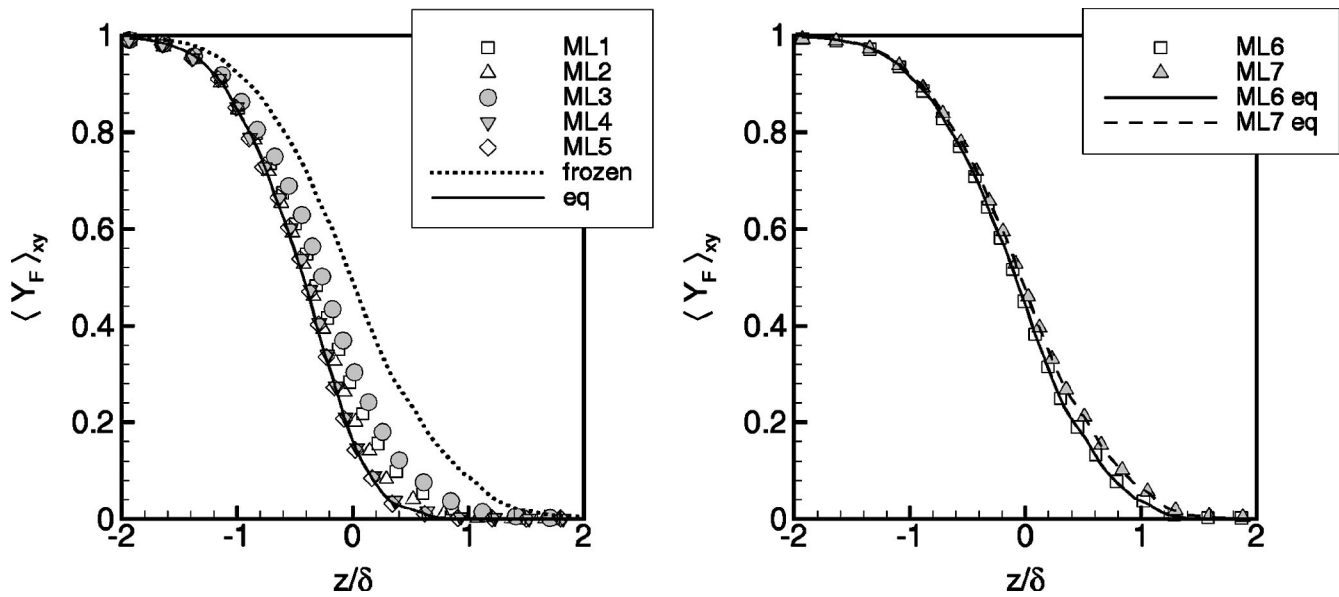
FIG. 7. Mean fuel mass fraction profiles at $x/M=231$. The frozen and equilibrium chemistry limits are denoted by ''frozen'' and ''eq,'' respectively.

only data at $x/M=231$ are presented except where it is particularly informative to observe the flow at other locations. Thus, the effects of Reynolds number on the various statistics are not evident from the data reported here, but the conclusions drawn are not contradicted by the data at other Reynolds numbers (from upstream locations in the simulations, or from the laboratory data). In the discussion which follows, the fluctuations of the fuel mass fraction about the planar mean ($\langle Y_F \rangle_{xy}$) are denoted y_F, i.e., $Y_F = \langle Y_F \rangle_{xy} + y_F$, and similarly for the fluctuations in Y_O.

A. Mean mass fractions

In Fig. 7, the profiles of the planar mean fuel mass fractions are plotted, along with the frozen and equilibrium limits for each of the different stoichiometries ($r=1,10,30$). The fuel mass fractions for finite rate chemistry must lie between the frozen and equilibrium chemistry limits, and one qualitative measure of the reaction rate is the deviation between the actual fuel profile and the two limits. From the plot, cases ML1 through ML5 span the range from near equilibrium to quite slow, which is consistent with the conclusions drawn from Fig. 3 and from the values of $\langle Da_T \rangle$ in Table II (case M3, M4, and M5 only).

As r is increased, the equilibrium limit for Y_F moves toward the frozen limit, and the equilibrium limit for Y_O, shown in Fig. 8, moves away from the frozen limit in the direction of the fuel-lean side of the mixing zone. This means that a fuel particle is moved further by turbulent advection, on average, before it is annihilated by oxidant when r is high than when it is low, and increasing r results in the reaction occurring where the gradient of the mixture fraction is, on average, lower. Thus, both the turbulent velocity and scalar molecular mixing time scales increase with increasing r, and the mean fuel and oxidant profiles will approach their equilibrium limits, which is the behavior observed in Figs. 7 and 8. The rate of product creation, however, goes down as r

increases, since it takes longer to mix the fuel and oxidant in stoichiometric proportions. The reduced Damköhler number ($\langle Da_T \rangle$) accounts for the decrease in the reaction rate due to increased r, as evidenced by the values in Table II for cases ML6 and ML7; both simulations have the same values of Da, but $\langle Da_T \rangle$ is lower for ML7 than for ML6. A lower Damköhler number for ML7 than for ML6 is consistent with the relative amount of extinction for each case, shown in Fig. 4. So, as r is increased, the reaction simultaneously becomes closer to the equilibrium limit, and closer to extinction, but produces product at a slower rate, a characteristic that is captured by $\langle Da_T \rangle$.

B. Profiles of the reactant fluctuations

In Fig. 9 are shown the profiles of the rms of the fluctuations in the fuel mass fraction, $y_{F_{rms}} = (\langle y_F^2 \rangle_{xy})^{1/2}$, along with the values for the equilibrium and frozen chemistry cases. Bilger *et al.*[1] note that there is no realizability con-
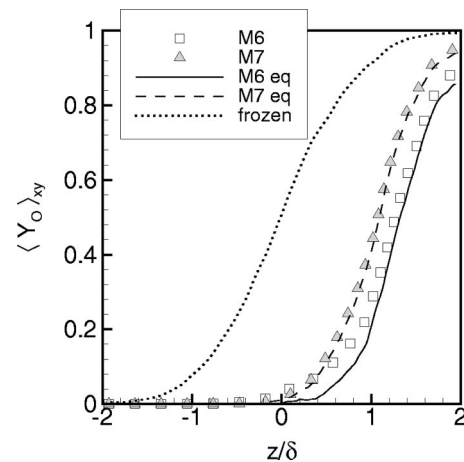

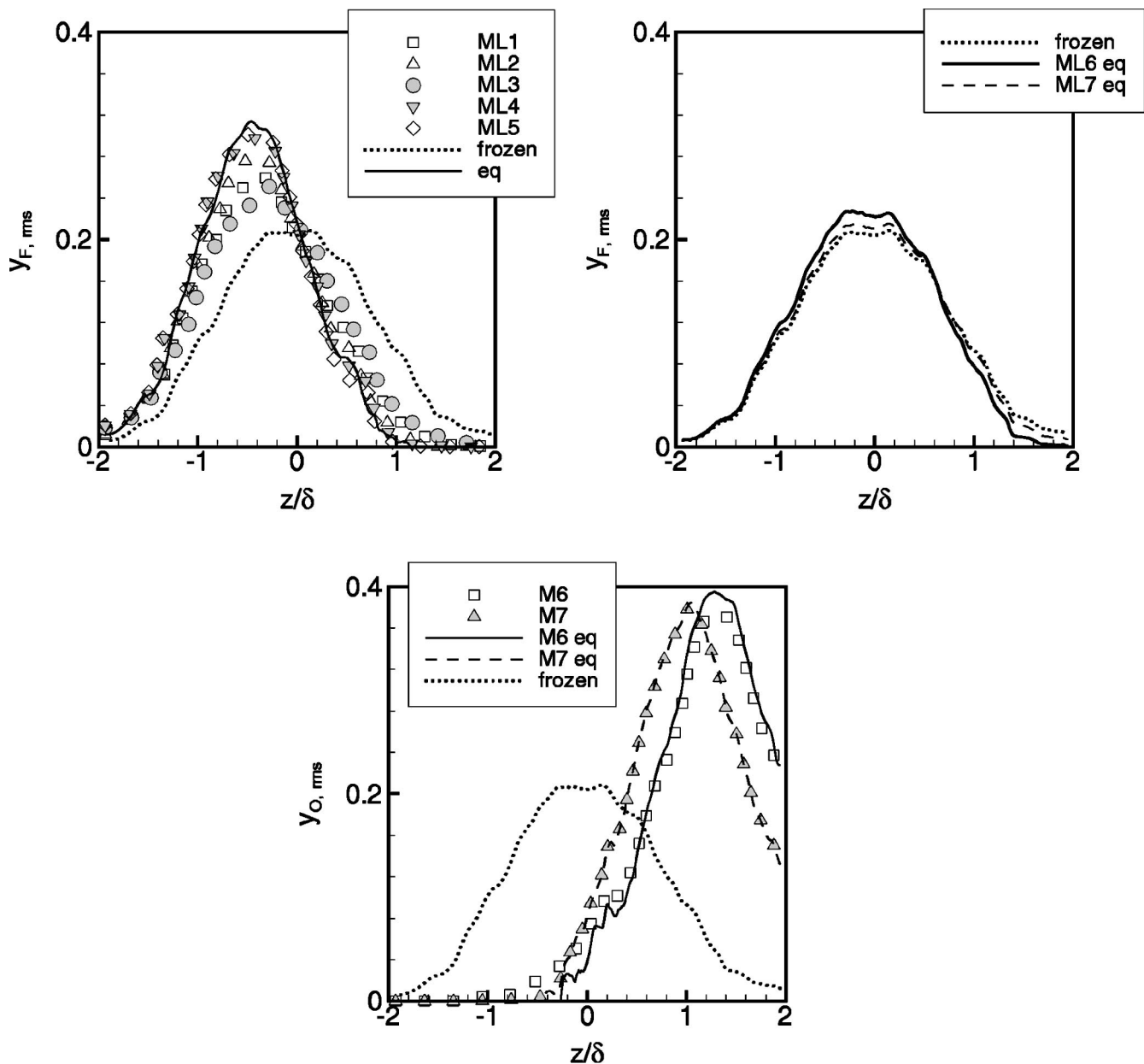FIG. 8. Mean oxidant mass fraction profiles at $x/M=231$.

FIG. 9. Profiles of the rms of the fluctuations in the fuel and oxidizer mass fraction at $x/M = 231$.

straint that the curves for the finite-rate reactions lie between the limiting cases, but that ''there appears to be a tendency for them to do so.'' Since the curves for the limiting reaction rates cross, they can only bound those for the finite rate cases in a qualitative sense. There is a distinct trend, however, in both the laboratory and simulation data for the rms profiles to resemble the equilibrium case when the reaction is fast, and to deviate from the equilibrium curve in the direction of the frozen curve when the reaction is slower.

For the cases with $r = 1$, the peak of the equilibrium chemistry fluctuation profile is about 50% higher than the peak of the frozen chemistry fluctuation profile, which is consistent with the laboratory results when the correction to the data noted in Bilger[17] is taken into account. When $r > 1$, the equilibrium, frozen, and finite rate fuel fluctuation profiles nearly coincide. The oxidizer fluctuation profiles for fi-

nite rate chemistry $(r > 1)$, shown in Fig. 9, nearly coincide with those of the equilibrium chemistry case, as might be expected from the behavior of the mean mass fraction profiles. The peaks of the oxidizer fluctuation profiles with $r > 1$ are approximately twice that of the frozen limit, and the large distance between the peak and the centerline of the mixing layer reflects the distance that fuel particles penetrate the oxidant stream. Based on the simple chemistry of these simulations, the fuel fluctuation profile could be accurately modeled by the frozen chemistry case, and the oxidizer fluctuation profile by the equilibrium case, when $r > 1$. When $r = 1$, the fluctuation profiles depend strongly on the reaction rate.

An additional observation can be made from Fig. 9 concerning how closely the simulations represent a canonical reacting scalar mixing layer. The numerical domain in the
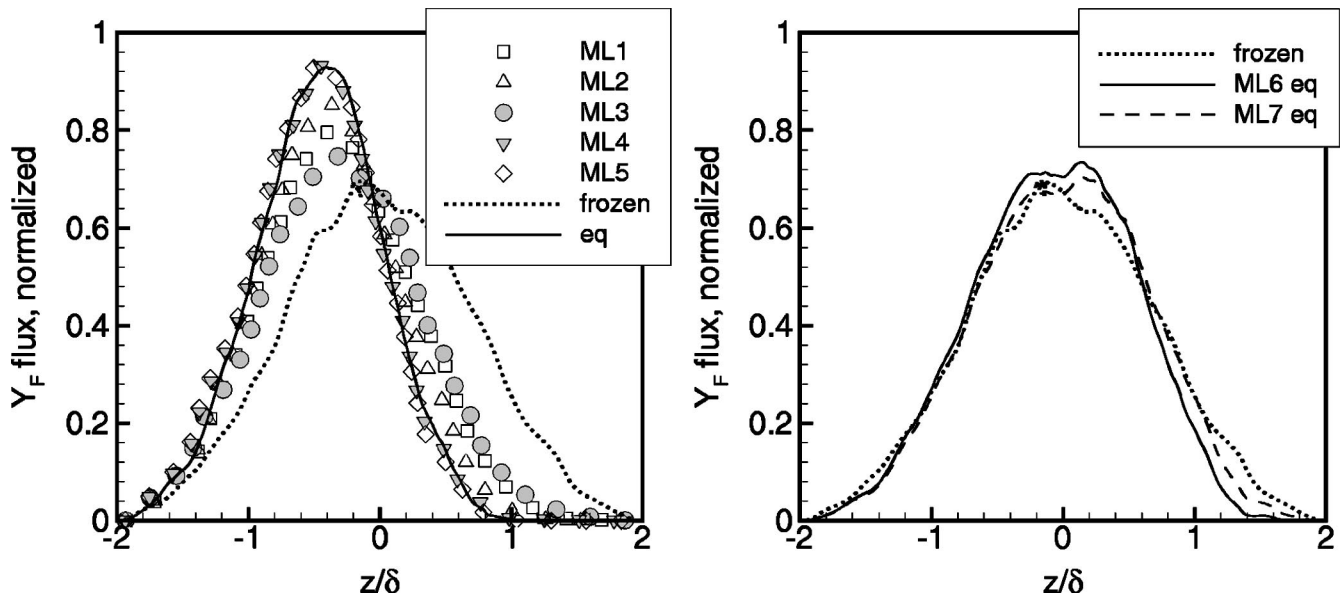
FIG. 10. Mean fuel mass fraction flux profiles at $x/M = 231$.

simulations is selected so that the mixing layer will not be significantly influenced by the boundary conditions (periodic or free slip) at $x/M = 231$, based on the mixture fraction field. The abscissa in the figure represents the full range of the transverse coordinate. Evidently, the oxidant mass fraction field is affected by the boundary conditions when $r > 1$, since fluctuations do not go to zero at the highest positive value of z/δ. This phenomenon is only observed in the far field and does not influence the results at upstream locations.

C. Fuel flux profiles

The fuel flux profiles, $\langle Y_F w' \rangle_{xy}/(w I_{max})$, where w' is the transverse fluctuating velocity, w is the rms of w', and I_{max} is the peak of average mixture fraction fluctuation profile, are exhibited in Fig. 10. (I_{max} vs x/M is shown in Fig. 5

of Ref 10. The value at $x/M = 231$ is 0.204. $w = w_{rms}$ is shown in Fig. 2.) The results for the isothermal cases are consistent with the laboratory data. As with the fluctuation profiles, when $r > 1$, the fuel flux profiles are very near that of the mixture fraction, and the oxidizer flux profiles (not shown) are almost identical to those in the equilibrium chemistry limit. Thus, both fluxes could be accurately modeled given only the mixture fraction. When $r = 1$, the profiles lie somewhere between the frozen and equilibrium cases, with the shape depending on the reaction rate.

D. Fuel-oxidizer covariance profiles

In Fig. 11, the covariance profiles of the fluctuating reactant mass fractions, $\langle y_F y_O \rangle_{xy}$, are displayed. When $r = 1$,
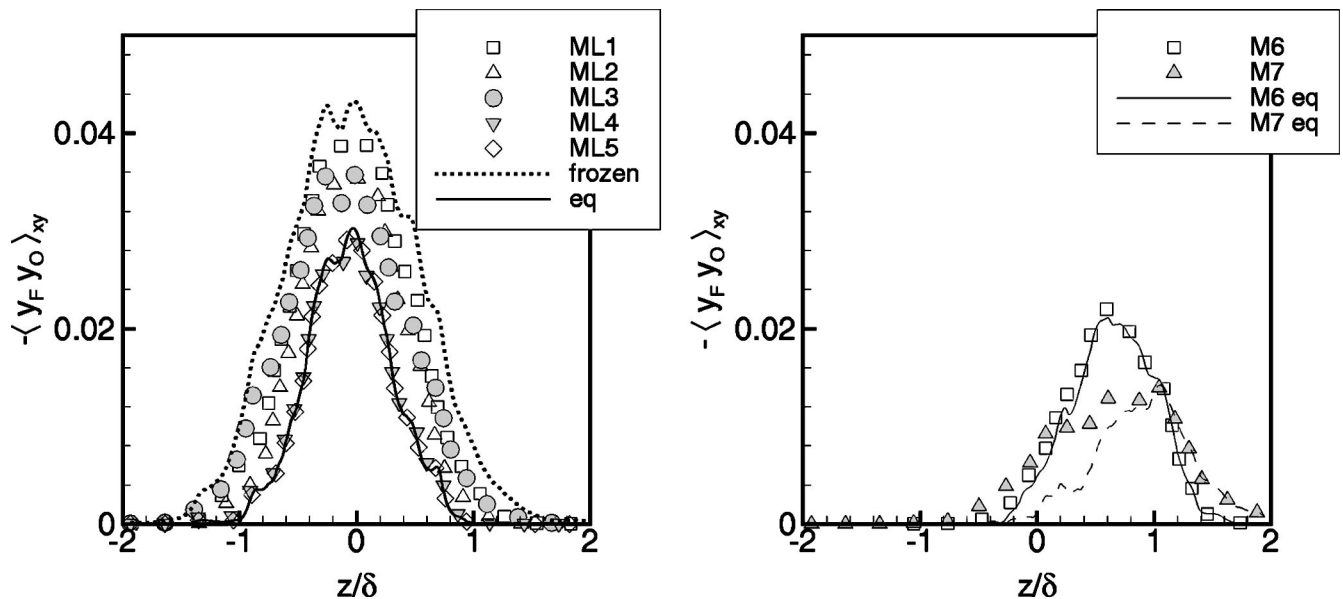

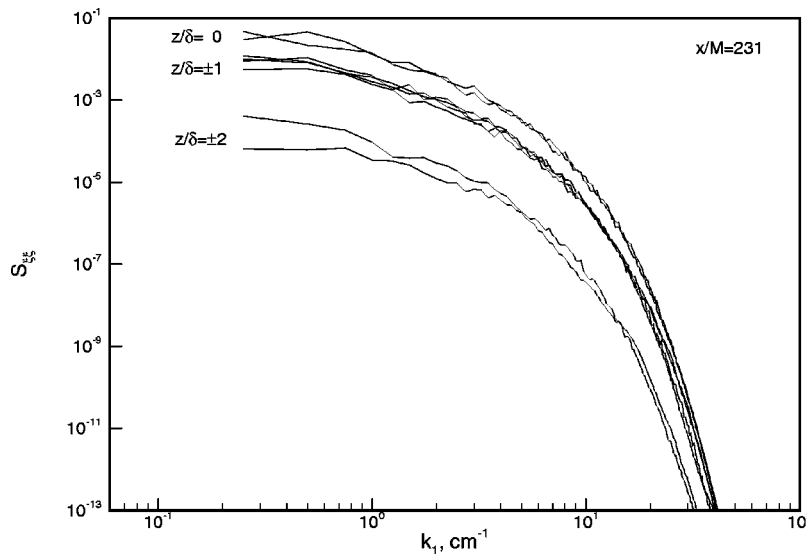FIG. 11. Mean covariance of the reactant mass fractions at $x/M = 231$.

FIG. 12. Autospectra of the conserved scalar at $x/M = 231$ and several cross-stream locations.

both the laboratory and simulation data show the covariance profiles monotonically changing from the frozen to the equilibrium chemistry shapes as the reaction rate increases. For $r > 1$, the profiles are similar to that with equilibrium chemistry. Toor[35] and Mudford and Bilger[36] propose equivalent models for the covariance of the reactants which equate it to the covariance of the equilibrium chemistry case, and Bilger et al.[1] note that interpolating between the frozen and equilibrium correlation limits of $\langle y_F y_O \rangle_{xy}$ might be an improvement for the cases they examined ($r = 1$). When $r > 1$, it appears from Fig. 11 that the equilibrium limit is a good model for the finite rate case.

E. Spectral density functions

Understanding the relationship between the spectral density functions (spectra) of reacting scalars and that of the mixture fraction would contribute significantly to turbulent combustion modeling,[37] and significant work has been done in this area by previous researchers.[3,22,37–39] Progress has been limited, however, by lack of data, with the two most recent papers cited relying heavily on the limited data from the Sydney experiments. The current data set provides scalar spectra at multiple downstream locations, as a function of the transverse coordinate, for the mixture fraction, for both of the reacting scalars in each of the seven chemistry cases, and for the equilibrium chemistry limit; this represents a substantial increase in the data available for study. Only a limited amount of these data is presented here.

The spectral density function is defined as in Bendat and Piersol.[40] Consider a scalar field, $\theta_1(x,y,z,t)$, with Fourier transform in the x direction

$$\hat{\theta}_1(k_x,y,z,t) = \int_{-\infty}^{\infty} \theta_1 \exp(-i2\pi k_x x) \, dx, \qquad (9)$$

and denote the complex conjugate of $\hat{\theta}_1$ as $\hat{\theta}_1^*$. Here, $i = \sqrt{-1}$ and k_x is the wave number in the x direction. In the simulations, it is convenient to average in the other homoge-

neous (y) direction in order to yield a spectrum that is function only of the transverse coordinate, time, and the wave number. Then, with y^+ and y^- the extreme values of the y coordinate, the cross spectrum of θ_1 and another scalar, θ_2, is

$$S_{\theta_1 \theta_2}(k_x,z,t) = \frac{1}{y^+ - y^-} \int_{y^-}^{y^+} \hat{\theta}_1^* \hat{\theta}_2 \, dy, \qquad (10)$$

which can also be written in terms of its magnitude and phase as

$$S_{\theta_1 \theta_2} = |S_{\theta_1 \theta_2}| \exp(-i\phi_{\theta_1 \theta_2}). \qquad (11)$$

The coherence between the scalar fluctuations is

$$C_{\theta_1 \theta_2} \equiv |S_{\theta_1 \theta_2}| / (S_{\theta_1 \theta_1} S_{\theta_2 \theta_2}), \qquad (12)$$

where $S_{\theta_1 \theta_1}$ and $S_{\theta_2 \theta_2}$ are the (real) autospectra of the two scalars.

We begin our study of the spectra by observing the autospectra of the conserved scalar at $x/M = 231$, which are shown in Fig. 12. In the computational domain with fully periodic boundary conditions there are two mixing layers, and each one is asymmetric about its respective $z/\delta = 0$. Therefore, the spectra computed from planes with equal $|z/\delta|$ are expected to have equal spectra as the size of the computational domain in x and y becomes indefinitely large. In Fig. 12, spectra from the two planes corresponding to $z/\delta = 0$ are shown, and the difference between them gives an indication of the scatter in the data. The four samples at $z/\delta = \pm 1$ demonstrate that each layer is asymmetric to within the scatter observed for $z/\delta = 0$. The final two curves correspond to $z/\delta = \pm 2$, where the layer exhibits intermittency in the scalar;[41] the relative difference between this pair of spectra is greater than between the spectra at $z/\delta = 0$ as significantly more scatter is expected in the highly intermittent region.
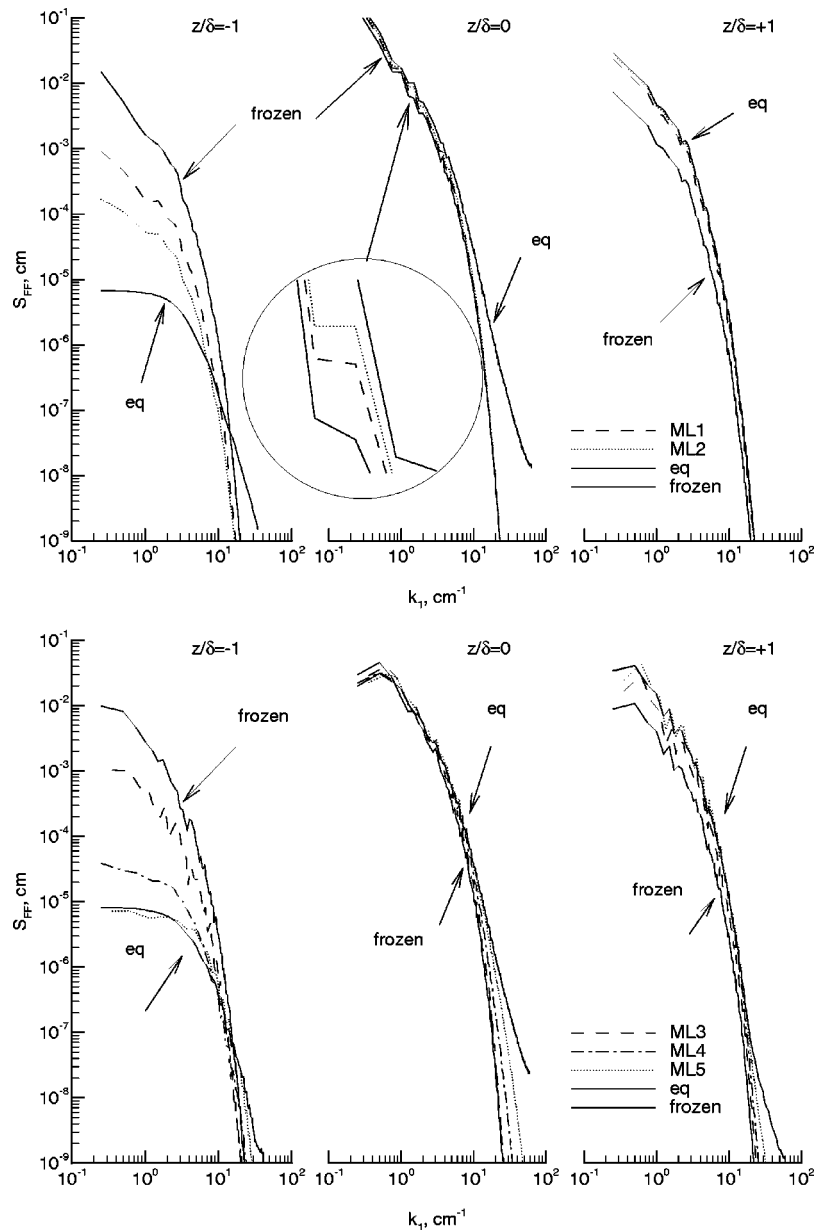
FIG. 13. Autospectra of the fuel mass fractions at $x/M = 231$ at three cross-stream locations for cases ML1, ML2, ML3, ML4, and ML5. (The top and bottom sets of figures are from two different realizations of the flow.)

Bilger[17] and Kosály[39] suggest that the mass fraction autospectra for the finite rate chemistry cases lies between the corresponding spectra in the frozen and equilibrium chemistry cases for the symmetric condition of $r = 1$ and $z/\delta = 0$; however, the spectrum for the equilibrium fuel mass fraction is not available from laboratory data in order to check this hypothesis. The fuel autospectrum for the equilibrium case can be computed from the DNS data, however, and it is displayed in Fig. 13 along with the corresponding spectra for frozen and intermediate reaction rates. At $z/\delta = 0$, the spectra trend monotonically from the frozen limit to the equilibrium limit as the Damköhler number of the reaction increases. This trend also holds on the fuel-rich side of the layer ($z/\delta = 1$). On the fuel-lean side of the layer ($z/\delta = -1$), only very small pockets of fuel exist, so the equilibrium spectra is lower than that for the frozen limit at larger scales, and the

spectra cross at some intermediate wave number. Nevertheless, the spectrum for the slow reaction (ML3) resembles that of the frozen limit, and the spectrum for the fast reaction (ML5) resembles that of the equilibrium limit.

In Fig. 14, the autospectra of the fuel and oxidant, along with the equilibrium and frozen limits, are shown for the cases in which $r > 1$ (ML6, ML7). In the top two plots, it is clear that the frozen, equilibrium, and finite rate fuel autospectra all nearly coincide; the autospectrum of the oxidizer (lower two plots) nearly coincides with the equilibrium limit. These findings are significant since they imply that both S_{FF} and S_{OO} can be predicted given $S_{\xi\xi}$ for reactions in which $r > 1$, even when $\langle Da_T \rangle$ is quite low, e.g., case ML7.

Kosály[39] explains in detail the phenomena observed in the laboratory data for the phase and coherence of the cross
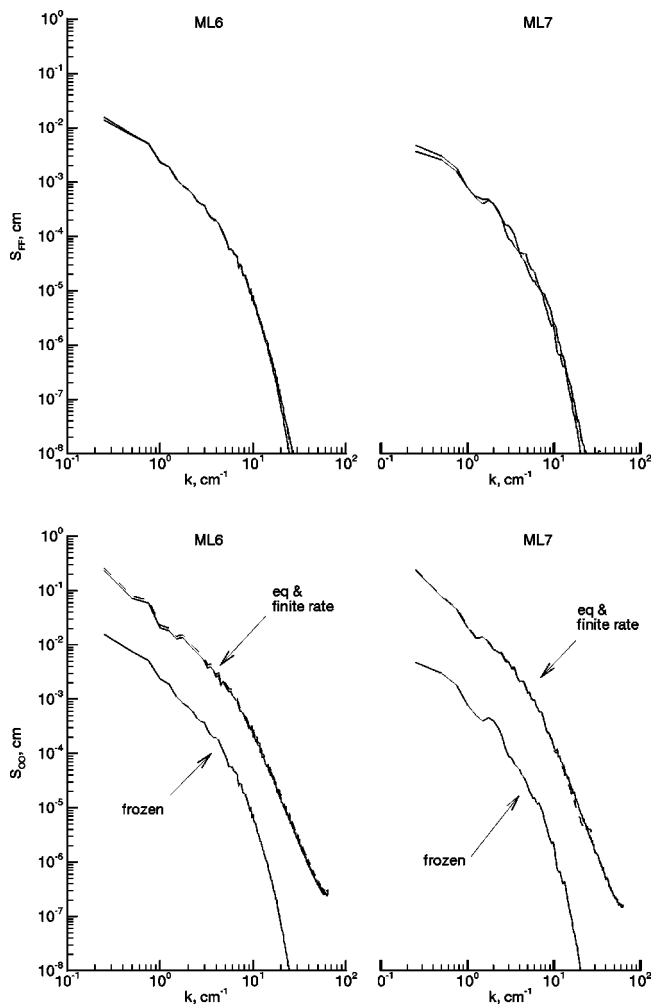
FIG. 14. The dashed lines are the autospectra of the fuel mass fractions at $x/M = 98$ averaged over the xy planes where $\langle \xi \rangle_{xy} = \xi_{st}$ for cases ML6 and ML7. The solid lines are the frozen and equilibrium limits.

FIG. 15. The phase and coherence of the cross spectra of the fuel and oxidant mass fractions, case ML4, at two downstream locations.

spectra of the fuel and oxidizer mass fractions. As in the laboratory data, the DNS results (Fig. 15) exhibit a 180° phase angle and high coherence at low wave numbers and low coherence with random phase at high wave number. In Fig. 15(a), data are shown at $x/M = 98$, where the numerical domain size is very large compared with the integral scale of the turbulence; this allows observation of the phase and coherence at very low wave numbers. As the flow develops, all the length scales increase, and the dynamic range decreases, so that by $x/M = 231$, relatively high wave numbers can be observed [Fig. 15(b)]. For frequencies higher than those recorded in the Sydney experiments, Kosály[39] predicts high coherence and 0° phase, which is also observed in Fig. 15. At the highest wave numbers available, the coherence decreases sharply in the case shown (ML4) and in the other cases, including those with isothermal reactions.

Finally, Kosály[39] develops a model for the autospectrum of the equilibrium fuel mass fraction in terms of the spectra of the mixture fraction and its absolute value. The principal assumption in the model is that the probability density function of the mixture fraction fluctuations can be approximated by a normal distribution; based on the data presented by de
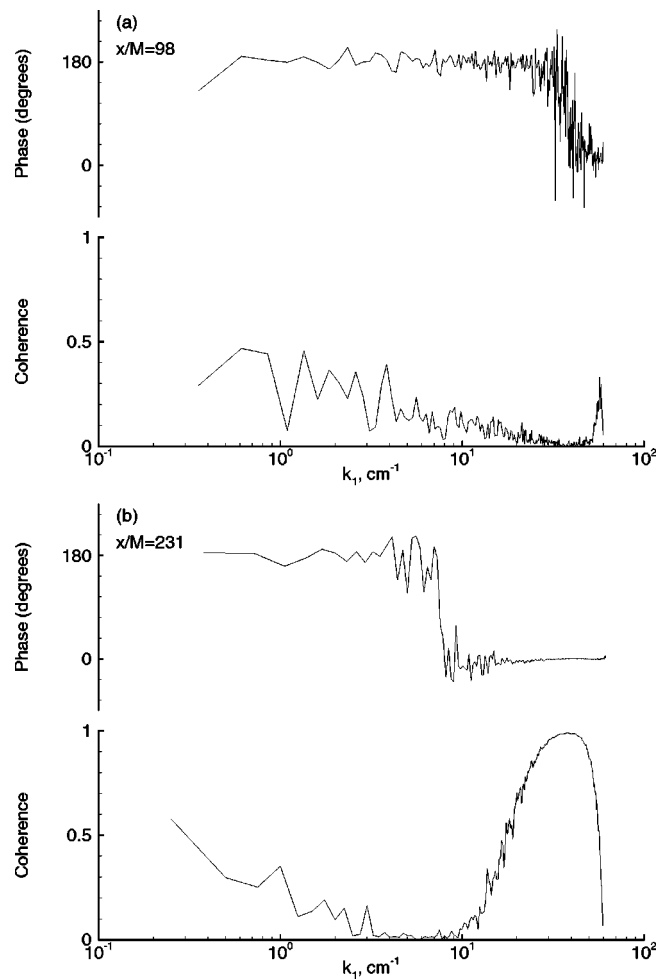
Bruyn Kops and Riley,[10] this assumption is good for the current simulations. It is not surprising, therefore, that the model predictions for the case of $r = 1$, shown in Fig. 16, closely agree with the results from the DNS.
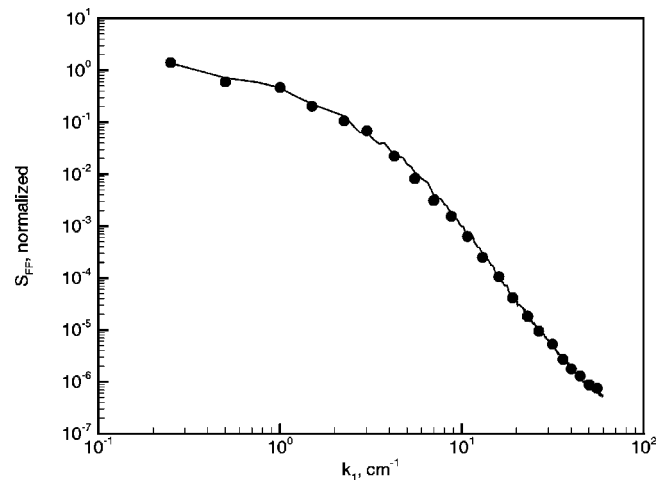

FIG. 16. Autospectrum of the equilibrium fuel mass fraction on centerline at $x/M = 231$ for $r = 1$, normalized by their respective variances. Symbols are the DNS data, line is the model prediction (Ref. 39).

VI. CONCLUSIONS

The reacting scalar mixing layer is a fundamental flow important to the understanding of non-premixed chemical reactions in turbulence. In this research, the flow is simulated by superimposing passive reactions on simulations of a thermal (nonreacting) mixing layer which has been closely matched to laboratory data. The reactions include isothermal and temperature dependent mechanisms. Numerical tests show that the simulation techniques used yield accurate solutions to the governing conservation equations and, for the two cases which are comparable to those measured in the laboratory at The University of Sydney ($r=1$, isothermal), the simulation and laboratory data are consistent. The simulations provide data on a reacting mixing layer which accurately represent the physical phenomena that occur in laboratory flows, and significantly increase the detail and scope of data that are available for studying the flow.

Several aspects of the reacting scalar mixing layer are investigated in this paper, and the following conclusions are drawn. First, it is observed that a reduced Damköhler number that includes the effects of temperature and stoichiometric mixture fraction[13–15] is a useful measure of the relative speed of the reaction. Second, research that focuses on reactions in which $r=1$ may exaggerate the difficulty in modeling statistics of the species mass fractions; the profiles of the mean, flux, covariance, and rms of the fluctuations in the fuel and oxidizer, as well as the autospectra of the reactants, can all be accurately modeled given the corresponding equilibrium and frozen limits for the cases studied in which $r>1$. Third, existing hypotheses concerning the coherence and phase of the fuel-oxidizer cross spectra[17,39] are shown to be correct for the current data. Fourth, a model developed by Kosály[39] to predict the equilibrium fuel autospectra from the mixture fraction yields excellent results for the current data.

ACKNOWLEDGMENTS

[1] R. W. Bilger, L. R. Saetran, and L. V. Krishnamoorthy, ''Reaction in a scalar mixing layer,'' J. Fluid Mech. **233**, 211 (1991).
[2] J. D. Li, R. J. Brown, and R. W. Bilger, ''Experimental study of a scalar mixing layer using reactive and passive scalars,'' in the 11th Australasian Fluid Mechanics Conference, Hobart, Australia, 1992, pp. 159–162.
[3] R. W. Bilger, in *Topics in Applied Physics Number 44: Turbulent Reacting Flows*, edited by P. A. Libby and F. A. Williams (Springer, New York, 1980), Chap. 3, pp. 65–113.
[4] W. E. Watt and W. D. Baines, ''The turbulent temperature mixing layer,'' J. Hydraul. Res. **11**, 158 (1973).
[5] P. A. Libby, ''Diffusion of heat downstream of a turbulence grid,'' Acta Astron. **2**, 867 (1975).
[6] J. C. LaRue and P. A. Libby, ''Thermal mixing layer downstream of half-heated turbulence grid,'' Phys. Fluids **24**, 597 (1981).
[7] J. C. LaRue, P. A. Libby, and D. V. R. Seshadri, ''Further results on the thermal mixing layer downstream of a turbulence grid,'' Phys. Fluids **24**, 1927 (1981).
[8] B.-K. Ma and Z. Warhaft, ''Some aspects of the thermal mixing layer in grid turbulence,'' Phys. Fluids **29**, 3114 (1986).
[9] M. M. Gibson, W. P. Jones, and V. E. Kanellopoulos, in *Turbulent Shear Flows 6*, edited by J.-C. Andre, J. Cousteix, F. Durst, B. Launder, F. Schmidt, and J. Whitelaw (Springer, New York, 1989), pp. 119–128.
[10] S. M. de Bruyn Kops and J. J. Riley, ''Re-examining the thermal mixing layer with numerical simulations,'' Phys. Fluids **12**, 185 (2000).
[11] P. A. Libby and F. A. Williams, *Turbulent Reacting Flows* (Academic, San Diego, 1994).
[12] F. A. Williams, *Combustion Theory: The Fundamental Theory of Chemically Reacting Flow Systems*, 2nd ed. (Benjamin–Cummings, Menlo Park, CA, 1985).
[13] A. Liñán, ''The asymptotic structure of counterflow diffusion flames for large activation energies,'' Acta Astron. **1**, 1007 (1974).
[14] B. Cuenot and T. Poinsot, ''Effects of curvature and unsteadiness in diffusion flames. Implications for turbulent diffusion combustion,'' in the *25th International Symposium on Combustion* (Combustion Institute, Pittsburgh, PA, 1994), pp. 1383–1390.
[15] B. Cuenot and T. Poinsot, ''Asymptotic and numerical study of diffusion flames with variable Lewis number and finite rate chemistry,'' Combust. Flame **104**, 111 (1996).
[16] G. K. Batchelor and A. A. Townsend, ''Decay of turbulence in the final period,'' Proc. R. Soc. London, Ser. A **194**, 527 (1948).
[17] R. W. Bilger, ''Conditional moment closure for turbulent reacting flow,'' Phys. Fluids A **5**, 436 (1993).
[18] S. M. de Bruyn Kops and J. J. Riley, ''Direct numerical simulation of laboratory experiments in isotropic turbulence,'' Phys. Fluids **10**, 2125 (1998).
[19] G. Comte-Bellot and S. Corrsin, ''Simple Eulerian time correlation of full and narrow-band velocity signals in grid-generated, 'isotropic' turbulence,'' J. Fluid Mech. **48**, 273 (1971).
[20] A. Sirivat and Z. Warhaft, ''The effect of a passive cross-stream temperature gradient on the evolution of temperature variance and heat flux in grid turbulence,'' J. Fluid Mech. **128**, 323 (1983).
[21] H. Tennekes and J. L. Lumley, *A First Course in Turbulence* (MIT, Cambridge, 1972).
[22] S. Corrsin, ''Further generalizations of Onsager's cascade model for turbulent spectra,'' Phys. Fluids **7**, 1156 (1964).
[23] N. Peters, ''Laminar diffusion flamelet models in non-premixed turbulent combustion,'' Prog. Energy Combust. Sci. **10**, 319 (1984).
[24] V. Eswaran and S. B. Pope, ''Direct numerical simulations of the turbulent mixing of a passive scalar,'' Phys. Fluids **31**, 506 (1988).
[25] W. H. Jou and J. J. Riley, ''Progress in direct numerical simulations of turbulent reacting flows,'' AIAA J. **27**, 1543 (1989).
[26] W. E. Mell, V. Nilsen, G. Kosály, and J. J. Riley, ''Investigation of closure models for turbulent reacting flow,'' Phys. Fluids **6**, 1331 (1994).
[27] C. J. Montgomery, ''Direct numerical simulation of turbulent nonpremixed hydrogen-oxygen combustion,'' Ph.D. thesis, University of Washington, 1995.
[28] S. Mahalingam, J. H. Chen, and L. Vervisch, ''Finite-rate chemistry and transient effects in direct numerical simulations of turbulent nonpremixed flames,'' Combust. Flame **102**, 285 (1995).
[29] N. Swaminathan and R. W. Bilger, ''Direct numerical simulation of turbulent nonpremixed hydrocarbon flames using a two-step reduced mechanism,'' Combust. Sci. Technol. **127**, 167 (1997).
[30] W. K. Bushe, R. W. Bilger, and G. R. Ruetsch, ''Direct numerical simulation of non-premixed combustion with realistic chemistry,'' J. Fluid Mech. (submitted).
[31] Y. Y. Lee and S. B. Pope, ''Nonpremixed turbulent reacting flow near extinction,'' Combust. Flame **101**, 501 (1995).
[32] L. Vervisch and T. Poinsot, in *Annual Review of Fluid Mechanics*, edited by J. L. Lumley, M. Van Dyke, and H. L. Reed (Annual Reviews, Palo Alto, CA, 1998), Vol. 30, pp. 655–691.
[33] V. Nilsen and G. Kosály, ''Differentially diffusing scalars in turbulence,'' Phys. Fluids **9**, 3386 (1997).
[34] V. Nilsen and G. Kosály, ''Differential diffusion in turbulent reacting flows,'' Combust. Flame **117**, 493 (1999).
[35] H. L. Toor, ''Turbulent mixing of two species with and without chemical reaction,'' Ind. Eng. Chem. Fundam. **8**, 655 (1969).

[36] N. R. Mudford and R. W. Bilger, ''Examination of closure models for mean chemical reaction using experimental data for an isothermal turbulent reacting flow,'' in the *20th International Symposium on Combustion* (Combustion Institute, Pittsburgh, PA, 1985), pp. 387–394.

[37] G. J. Sabini, G. S. Shieh, and P. Givi, ''Modeling of the fluctuations and the frequency-spectra of reactants in turbulent scalar mixing layers,'' Chem. Eng. Commun. **154**, 147 (1996).

[38] S. Corrsin, ''The reactant concentration spectrum in turbulent mixing with a first order reaction,'' J. Fluid Mech. **11**, 407 (1961).

[39] G. Kosály, ''Frequency spectra of reactant fluctuations in turbulent flows,'' J. Fluid Mech. **246**, 489 (1993).

[40] J. S. Bendat and A. G. Piersol, *Engineering Applications of Correlation and Spectral Analysis* (Wiley, New York, 1980).

[41] J. F. Keffer, G. J. Olsen, and J. G. Kawall, ''Intermittency in a thermal mixing layer,'' J. Fluid Mech. **79**, 595 (1977).